Winter Weather Regimes in the Northeast United States

Christopher D. Roller, Jian-Hua Qian, Laurie Agel, Mathew Barlow, Vincent Moron

Winter Weather Regimes in the Northeast United States

CHRISTOPHER D. ROLLER AND JIAN-HUA QIAN

Department of Environmental, Earth, and Atmospheric Sciences, University of Massachusetts Lowell, Lowell, Massachusetts

LAURIE AGEL

Department of Environmental, Earth, and Atmospheric Sciences, and Intercampus Marine Science Graduate Program, University of Massachusetts Lowell, Lowell, Massachusetts

MATHEW BARLOW

Department of Environmental, Earth, and Atmospheric Sciences, and Climate Change Initiative, University of Massachusetts Lowell, Lowell, Massachusetts

VINCENT MORON

Aix-Marseille University, CEREGE, UM 34 CNRS, Aix en Province, France

(Manuscript received 17 April 2015, in final form 23 January 2016)

ABSTRACT

The method of *k*-means cluster analysis is applied to U.S. wintertime daily 850-hPa winds across the Northeast. The resulting weather patterns are analyzed in terms of duration, station, gridded precipitation, storm tracks, and climate teleconnections. Five distinct weather patterns are identified. Weather type (WT) 1 is characterized by a ridge over the western Atlantic and positive precipitation anomalies as far north as the Great Lakes; WT2, by a trough along the eastern United States and positive precipitation anomalies into southern New England; WT3, by a trough over the western Atlantic and negative precipitation anomalies along much of the U.S. East Coast; WT4, by a trough east of Newfoundland and negative precipitation anomalies along parts of the U.S. East Coast; and WT5, by a broad, shallow trough over southeastern Canada and negative precipitation anomalies over the entire U.S. East Coast. WT5 and WT1 are the most persistent, while WT2 typically progresses quickly to WT3 and then to WT4. Based on mean station precipitation in the northeastern United States, most precipitation occurs in WT2 and WT3, with the least in WT1 and WT4. Extreme precipitation occurs most frequently in WT2. Storm tracks show that WT2 and WT3 are associated with coastal storms, while WT2 is also associated with Great Lakes storms. Teleconnections are linked with a change in WT frequency by more than a factor of 2 in several cases: for the North Atlantic Oscillation (NAO) in WT1 and WT4 and for the Pacific–North American (PNA) pattern in WT1 and WT3.

1. Introduction

Weather type (WT) analysis is a way to objectively and compactly describe the climatology of main weather patterns for a region. It can be used as a basis for understanding a broad scale of relationships such as flow patterns and the influence of teleconnections on those patterns, as well as the progression from one weather pattern to another. A common method of isolating weather patterns involves the *k*-means clustering technique (Diday and Simon 1976; Ghil and Robertson 2002).

The goal of this paper is to objectively determine the primary daily circulation patterns over the northeastern United States during winter, and to examine their links to known teleconnections, synoptic regimes, and precipitation. We use *k*-means clustering to determine these patterns, which, given the daily time scale, we refer to as "weather types." The *k*-means technique has

Corresponding author address: Jian-Hua Qian, Department of Environmental, Earth, and Atmospheric Sciences, University of Massachusetts Lowell, One University Avenue, Lowell, MA 01854.
E-mail: jianhua_qian@uml.edu

DOI: 10.1175/JCLI-D-15-0274.1

previously been shown to be useful in isolating circulation patterns (Lana and Fernandez-Mills 1994; Sheridan 2002; Stahl et al. 2006; Coleman and Rogers 2007a,b; Boé and Terray 2008), although it has not yet been applied to the northeastern United States. Objectively defined WTs are useful in a range of applications, including providing a context for dynamical analysis (Straus et al. 2007; Moron et al. 2010; Qian et al. 2010), serving as the basis for downscaling (Conway and Jones 1998; Moron et al. 2008; Demuzere et al. 2009), examining weather-relevant trends and projections (Riddle et al. 2013), and providing a basis for evaluating climate models (Perez et al. 2014). Persistence and/or transitioning of weather types can also be used in subseasonal to seasonal climate variability and predictability studies, linking weather and climate (Coleman and Rogers 2007a).

Here, we use WTs to better understand the link between synoptic patterns in the U.S. Northeast and the larger-scale circulation. Extratropical storms play a significant role in generating these synoptic patterns; although Northeast storms have been analyzed in a number of contexts (e.g., Stuart and Grumm 2006; Notaro et al. 2006; Archambault et al. 2010), a WT analysis, which provides an objective categorization and considers all days, has not yet been done. We use the WTs to identify patterns that are most likely to generate extreme precipitation, and we analyze the persistence and transitioning between the WTs to better understand the bridge between synoptic-scale and large-scale influences. The link between the WTs and large-scale circulation regimes is explored by investigating the relationship of each WT to several important climate teleconnections: the North Atlantic Oscillation (NAO), Arctic Oscillation (AO), Pacific–North American (PNA) pattern, and El Niño–Southern Oscillation (ENSO). A brief summary of the teleconnections and their links to Northeast weather follows.

The NAO pattern (Barnston and Livezey 1987) is based on out-of-phase variations of sea level pressure (SLP) or 500-hPa geopotential height anomalies between subpolar low pressure located over Greenland or Iceland and subtropical Azores high pressure between 35° and 40°N. The positive (negative) phase occurs when lower (higher) than normal heights and pressure occur in the North Atlantic and higher (lower) than normal heights and pressure occur over the central North Atlantic, eastern United States, and western Europe. The pressure and height anomalies influence the location and orientation of the North Atlantic jet stream, which in turn influences storm-track locations over the North Atlantic basin. Jones and Davis (1995) demonstrated that a negative NAO increases the frequency of nor'easters. Archambault et al. (2010) showed that a transition from positive to negative NAO may be associated with the occurrence of storms, and Serreze et al. (1997) noted that there are a greater number of storms coincident with Icelandic low pressure systems.

The daily AO pattern is based on the projection of daily 1000-hPa height anomalies poleward of 20°N onto the leading empirical orthogonal function (EOF) mode of 1000-hPa monthly mean height anomalies. The positive (negative) phase occurs when lower (higher) than normal pressure occurs in the polar region and above (below)-normal pressure occurs around latitude 45°N, resulting in a stronger (weaker) polar vortex. In the positive (negative) phase, storm tracks are shifted north (south) as the jet stream moves northward (southward) and becomes stronger (weaker) (Rohli and Vega 2008).

The PNA pattern (Barnston and Livezey 1987) is based on 500-hPa height anomalies over the North Pacific and North America and is related to the variability in strength and location of the East Asian jet stream. In the positive (negative) phase, a stronger (weaker) East Asian jet stream exit region is shifted eastward (westward) in relation to eastern Asia. In the northeastern United States, the positive (negative) PNA phase is related to lower (higher) height anomalies. Leathers et al. (1991) found that there is a correlation between the PNA and Northeast temperature and some correlation between the PNA and Northeast precipitation. Notaro et al. (2006) also found a connection between Northeast precipitation and the PNA. However, Bradbury et al. (2002) found no discernable connection between the PNA and Northeast wintertime precipitation, temperature, and snowfall.

ENSO is a mode of coupled variability between Pacific trade winds and ocean temperature (Rasmusson and Carpenter 1982) that has global weather impacts (e.g., Ropelewski and Halpert 1987). The warm phase (El Niño) features a more eastward extension of warm waters toward the eastern Pacific, along with a stronger than normal subtropical jet due to an eastward shift of subtropical high pressure (Eichler and Higgins 2006), whereas the cold phase (La Niña) features a stronger than normal upwelling of cold waters in the eastern Pacific (Rohli and Vega 2008). The resulting warm (in warm phase) or cold (in cold phase) water temperature anomalies just southwest of the U.S. West Coast can affect downstream large-scale atmospheric flow. However, there has been some disagreement as to the overall effects of ENSO on the northeastern United States. Several studies have suggested no clear link to New England climate (Ropelewski and Halpert 1986; Kahya and Dracup 1993; Piechota and Dracup 1996), while others have suggested that El Niño is linked to more East Coast storms (Hirsch et al. 2001),

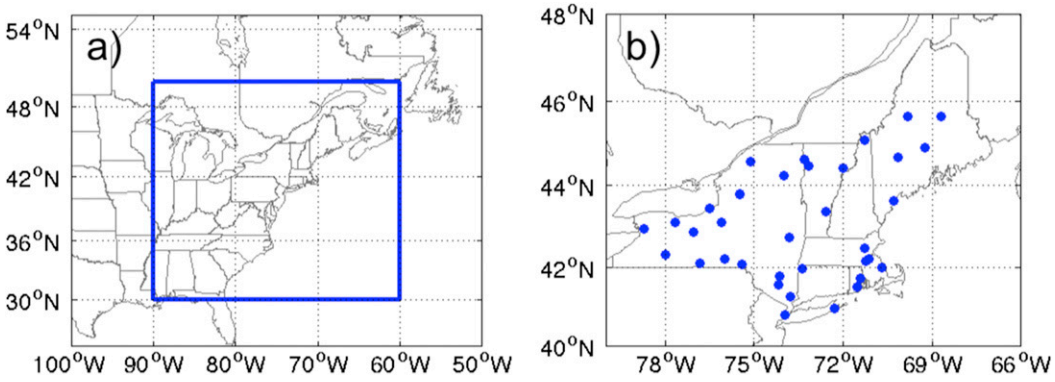

FIG. 1. Maps showing the (a) boundaries of the Northeast region used to subset MERRA 850-hPa winds for input to the *k*-means clustering algorithm, and (b) locations of the USHCN stations used for precipitation analysis and storm-track analysis.

more heavy snow (Patten et al. 2003), more Gulf of Mexico cyclones, and fewer Alberta clippers (Kunkel and Angel 1999). La Niña has been linked to low pressure systems over central western Canada (Rogers 1984; Trenberth and Caron 2000; Bradbury et al. 2003) and more storm tracks in the Midwest and St. Lawrence regions (Kunkel and Angel 1999). Great Lakes ice cover also appears to be affected, with the largest ice cover occurring in neutral ENSO years (Bai et al. 2010).

The remainder of this paper is organized as follows. In section 2, we describe the data used and the *k*-means clustering method that generates the wintertime WTs for the northeastern United States. In section 3, we describe each resulting WT pattern in terms of 850-hPa winds and gridded precipitation, analyze the tendency of each pattern to persist or transition to other patterns, and evaluate the WTs in terms of their relationship to station precipitation and extreme precipitation, storm tracks, and teleconnections. In section 4, we summarize and discuss the results.

2. Data and methods

a. Data

The National Aeronautics and Space Administration (NASA) Modern-Era Retrospective Analysis for Research and Applications (MERRA; Rienecker et al. 2011; NASA 2014) daily 850-hPa zonal u and meridional v component winds for December–February (DJF) during 1981–2010 are used as input to the *k*-means clustering algorithm. The region used for analysis is bounded by 30°–50°N latitude and 60°–90°W longitude (Fig. 1a). The winds are standardized by removing the long-term DJF mean and dividing by the standard deviation, and the resulting dataset is then reduced through EOF analysis to retain 75% of the total variance before running the *k*-means analysis. The EOF compression reduces the degrees of freedom to make the problem more computationally efficient. Standardization of the data before EOF analysis allows small-scale variability in the wind fields to be on an equal footing with large-scale circulation variability. The 850-hPa level was chosen since it is above the mountainous regions in the Northeast but as close to the ground as possible to be able to resolve low pressure systems. To validate the representativeness of the 850-hPa winds, we also performed *k*-means clustering separately on MERRA daily mean sea level pressure (MSLP) and 500-hPa geopotential heights, as well as on a combination of these three variables.

Gridded precipitation data are from the Precipitation Estimation from Remotely Sensed Information Using Artificial Neural Networks–Climate Data Record (PERSIANN-CDR; Ashouri et al. 2015; NCDC 2015). PERSIANN-CDR is extracted from gridded satellite (GridSat-B1) infrared data using artificial neural networks and bias corrected using monthly GPCP 2.5° × 2.5° precipitation. The final product is available at 0.25° × 0.25° daily resolution from 1983 to near present, and provides a long-term consistent dataset.

In addition to gridded data, station precipitation from the National Climatic Data Center (NCDC) U.S. Historical Climatology Network (USHCN; Easterling et al. 1999) is used. This set includes high-quality daily data from U.S. Cooperative Observer Program stations and several National Weather Service first-order stations. Northeast stations missing less than 1% of the daily precipitation data for the period of 1980–2010 are used in the analysis (Fig. 1b).

Storm-track data (T. Eichler 2012, unpublished manuscript) are based on a modification of the Serreze (1995) and Serreze et al. (1997) scheme that uses

6-hourly National Centers for Environmental Prediction (NCEP)–U.S. Department of Energy (DOE) AMIP-II reanalysis (Kanamitsu et al. 2002) sea level pressure to identify cyclone centers. The data are interpolated onto a 250 km × 250 km version of the National Snow and Ice Data Center (NSIDC) Equal-Area Scalable Earth Grid (EASE-Grid; Armstrong and Brodzik 1995). Storm tracks for the period of 1980–2008 are used.

The teleconnection indices used include the daily NAO, PNA, and the AO indices from the Climate Prediction Center (CPC; ftp://ftp.cpc.ncep.noaa.gov/cwlinks), and the seasonal Niño-3.4 index (Reynolds et al. 2002) also from the CPC (http://www.cpc.ncep.noaa.gov/data/indices).

b. The k-means clustering method

The k-means clustering algorithm follows that of Diday and Simon (1976). The procedure of k-means clustering seeks to find a partitioning of data into a predetermined number of clusters k that minimizes the function W:

$$W(P) = \sum_{j=1}^{N} \sum_{x \in C_j} d^2(X, Y_j), \tag{1}$$

where P represents a particular partitioning of the data into a set of k clusters $C_1, C_2, \ldots, C_k$; Y_j is the centroid of cluster C_j; $d(X, Y_j)$ is the Euclidean distance between points X in C_j and the centroid Y_j; and $W(P)$ signifies the intracluster sum of variance for a particular partitioning. The global minimum of the function $W(P)$ represents the partition that achieves the best separation of the data points into the k clusters. The process of finding the minimum $W(P)$ is iterative, and is accelerated by choosing initial centroids from a small subset of the data first.

The classifiability index (CI; Michelangeli et al. 1995) is used to determine the minimum number of clusters k required to achieve adequate separation of the data. The CI depends on the anomaly correlation coefficients (ACC) between partition clusters. The ACC between two partition clusters P_i and Q_j is defined as shown:

$$\mathrm{ACC}\,(P_i, Q_j) = \frac{\sum_{n=1}^{N} p'_n q'_n}{\sqrt{\sum_{N=1}^{N} (p'_n)^2 \sum_{n=1}^{N} (q'_n)^2}},$$

$$p'_n = p_n - \frac{\sum_{n=1}^{N} p_n}{N}, \quad \text{and}$$

$$q'_n = q_n - \frac{\sum_{n=1}^{N} q_n}{N}, \tag{2}$$

where $1 \le i, j \le k$, $P \ne Q$, and p_n and q_n are the centroids of clusters in the partitions P_i and Q_j, respectively. When the two partitioned clusters are identical, the ACC is 1. As in Moron et al. (2010), an "ACC score" is assigned to each cluster P_i: this is the maximum ACC between P_i and each cluster Q_j in partitions $Q \ne P$, where $j = 1, \ldots, k$, averaged over all Q partitions. Given N partitions, there are then $N \times k$ ACC scores. The CI for a partitioning into k clusters is then defined as the average of the ACC scores, and the individual partition with the maximum ACC score represents the best separation of the data into the k clusters. To determine the minimum number of clusters required to achieve adequate separation of the data, CI is calculated for several values of k. For each value of k, the k-means algorithm is also run numerous times using random red noise generated from the data, in order to create a range of CI values attributable to chance. The optimum number of clusters is the minimum k with a CI above 90% of CI values due to random red noise (Michelangeli et al. 1995).

In this study, k is varied from 2 to 10 clusters for each of 100 different partitions created from randomly chosen initial seeds. The CI increases as the number of partitions becomes large; however, using more partitions slows the computation speed for each cluster. Here, 100 partitions is deemed acceptable to achieve stable CI values. Figure 2a shows the CIs that result from k-means clustering of 2–10 clusters. The gray shading indicates the bottom 90% of CIs for random red noise generated from the data. Based on the CI value in relation to those due to red noise, the 850-hPa winds can be reasonably separated into $k = 5$ distinct clusters, or patterns.

3. Results

a. Weather types

The k-means clustering algorithm is applied to MERRA daily 850-hPa u- and v-component winds for DJF 1981–2010 (standardized and reduced through EOF analysis to retain 75% of variance) within the region specified in Fig. 1a. The data are separated into five clusters (based on the relative CI value from Fig. 2a), with each day assigned to a single cluster. Each cluster represents a pattern, or weather type. The relative frequency of each WT is shown in Fig. 2b. Each WT comprises ~15%–25% of the DJF days, with WT2 (14%) having the least number of days and WT5 (26%) having the greatest number of days. The relative frequency of WTs per month (not shown) is similar to that for the entire DJF period, with the exception of slightly more

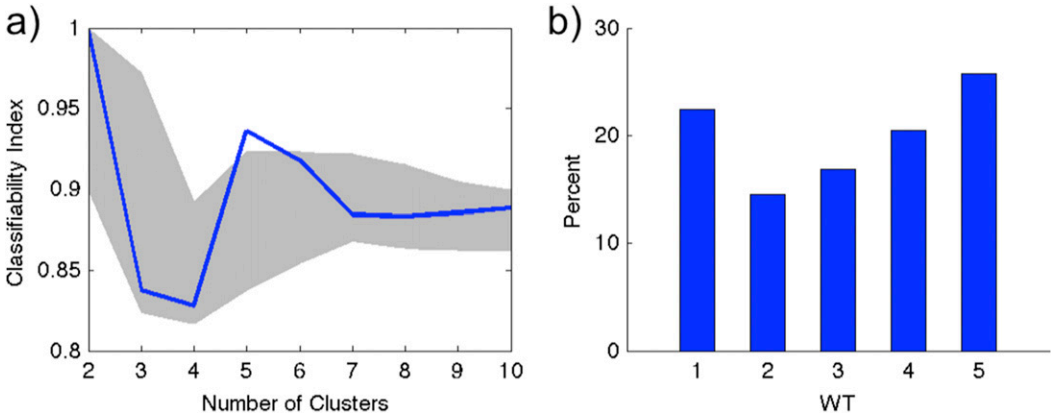

FIG. 2. Results of *k*-means clustering applied to MERRA 850-hPa winds for DJF 1981–2010. The figure shows the (a) CI for various numbers of clusters (blue solid line) and the one-sided 90% confidence interval of the CI due to random noise (gray shading), suggesting 5 as the optimal number of clusters; and (b) percent of days assigned to each cluster or WT, representing the ''background frequency'' of the WTs.

WT1 days in December and slightly more WT4 days in February.

The WTs are shown in Figs. 3 and 4. WT composites of DJF 850-hPa winds and PERSIANN-CDR gridded precipitation are shown in Figs. 3a–e, and the DJF 30-yr mean is shown in Fig. 3f. In WT1, a trough is present over the central United States with a ridge located just off the East Coast (''coastal ridge'' type). The Northeast experiences little precipitation and light southwest winds, while stronger southwest winds transport moisture

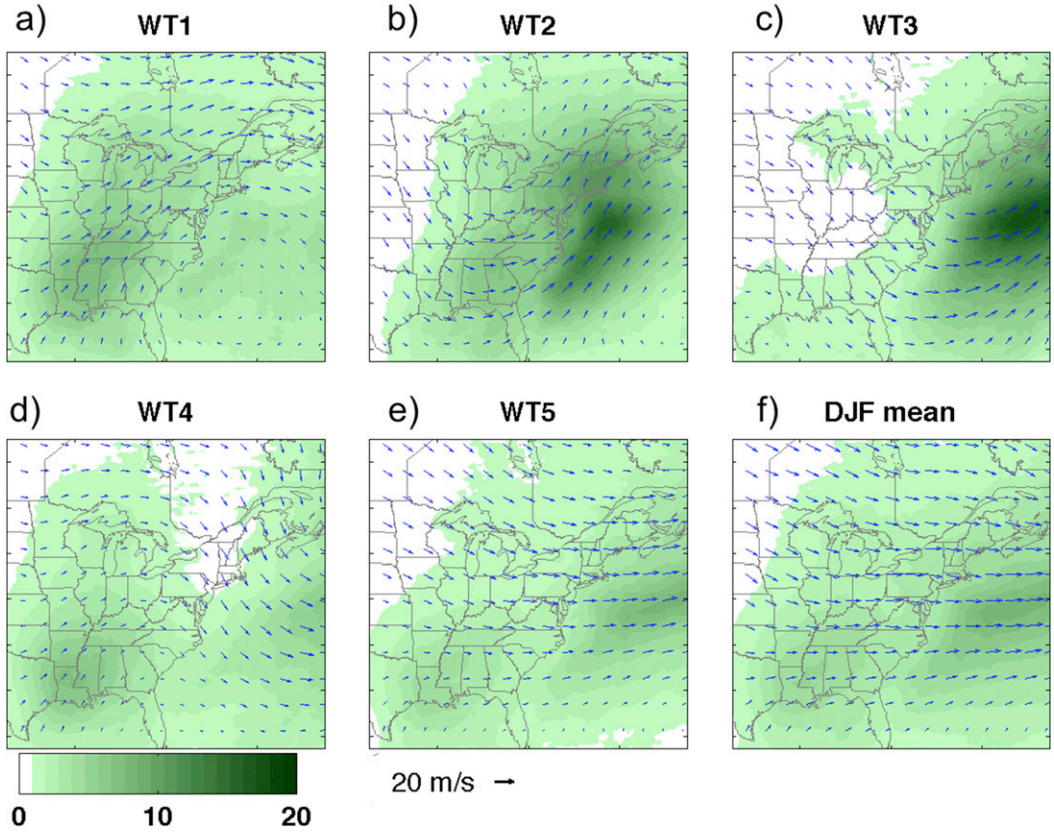

FIG. 3. MERRA 850-hPa winds for DJF 1981–2010 (vectors) and PERSIANN-CDR precipitation for DJF 1983–2010 (shaded; mm day^{-1}) for (a) WT1, (b) WT2, (c) WT3, (d) WT4, (e) WT5, and (f) the 30-yr DJF mean.

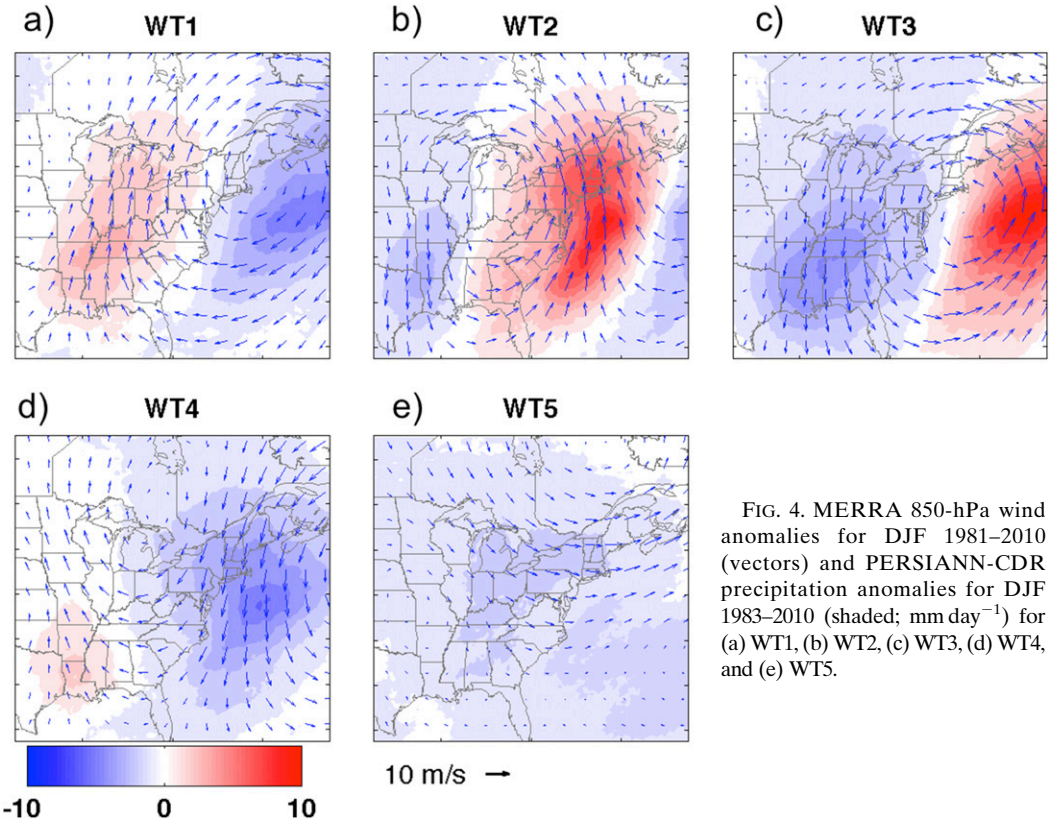

FIG. 4. MERRA 850-hPa wind anomalies for DJF 1981–2010 (vectors) and PERSIANN-CDR precipitation anomalies for DJF 1983–2010 (shaded; mm day^{-1}) for (a) WT1, (b) WT2, (c) WT3, (d) WT4, and (e) WT5.

from the Gulf of Mexico to the southeastern United States, generating light to moderate precipitation. WT2 exhibits a large trough between the Midwest and East Coast with a ridge to the west (''coastal land trough'' type). This WT generates the highest amount of precipitation in the eastern United States, including the Northeast, due to a low-level jet just offshore carrying moisture from the southern United States and the Gulf Stream. WT3 experiences dominant northwest flow and light precipitation over the eastern United States. However, a trough located offshore (''coastal ocean trough'' type) generates significant precipitation in the western Atlantic. In WT4, a ridge exists over the southeastern United States and a trough exists offshore (''mid–Atlantic Ocean trough'' type), resulting in northwest winds and little precipitation over the Northeast. Southwest winds bring precipitation into the southern United States as for WT1, but a weaker 850-hPa low-level jet keeps the precipitation farther south. WT5 exhibits a zonal flow with confluence in the mid-Atlantic region of the United States (''zonal flow'' type). The Northeast experiences little precipitation under the northwesterly winds, while the southeastern United States experiences light precipitation in weak southwest winds. The DJF mean is similar to WT5, with predominant westerlies, confluent flow through the mid-Atlantic, light precipitation to the north, and heavier precipitation to the south. This is not surprising since it represents both the canceling effects of out-of-phase synoptic systems in WT1–WT4 as well as the frequent zonal flow WT5 pattern.

A complementary view of the WTs can be seen using composites of anomalous (long-term daily mean removed) 850-hPa winds and precipitation (Fig. 4). In addition, the standard deviations of the u- and v-wind components are shown in Fig. 5. WT1 has high pressure just off the southern New England coast, and strong southerly flow into the eastern United States. The highest positive precipitation and wind anomalies occur over the Midwest. WT2 has low pressure over the Midwest, which leads to anomalously strong southerly flow into the Northeast. The warm moist air associated with this anomalously strong low-level southerly flow likely contributes to the heavy precipitation in this WT. On the other hand, WT3 depicts low pressure off the coast of New Jersey, with anomalously strong easterly winds along the New England coast, leading to the possibility of strong moisture advection due to the

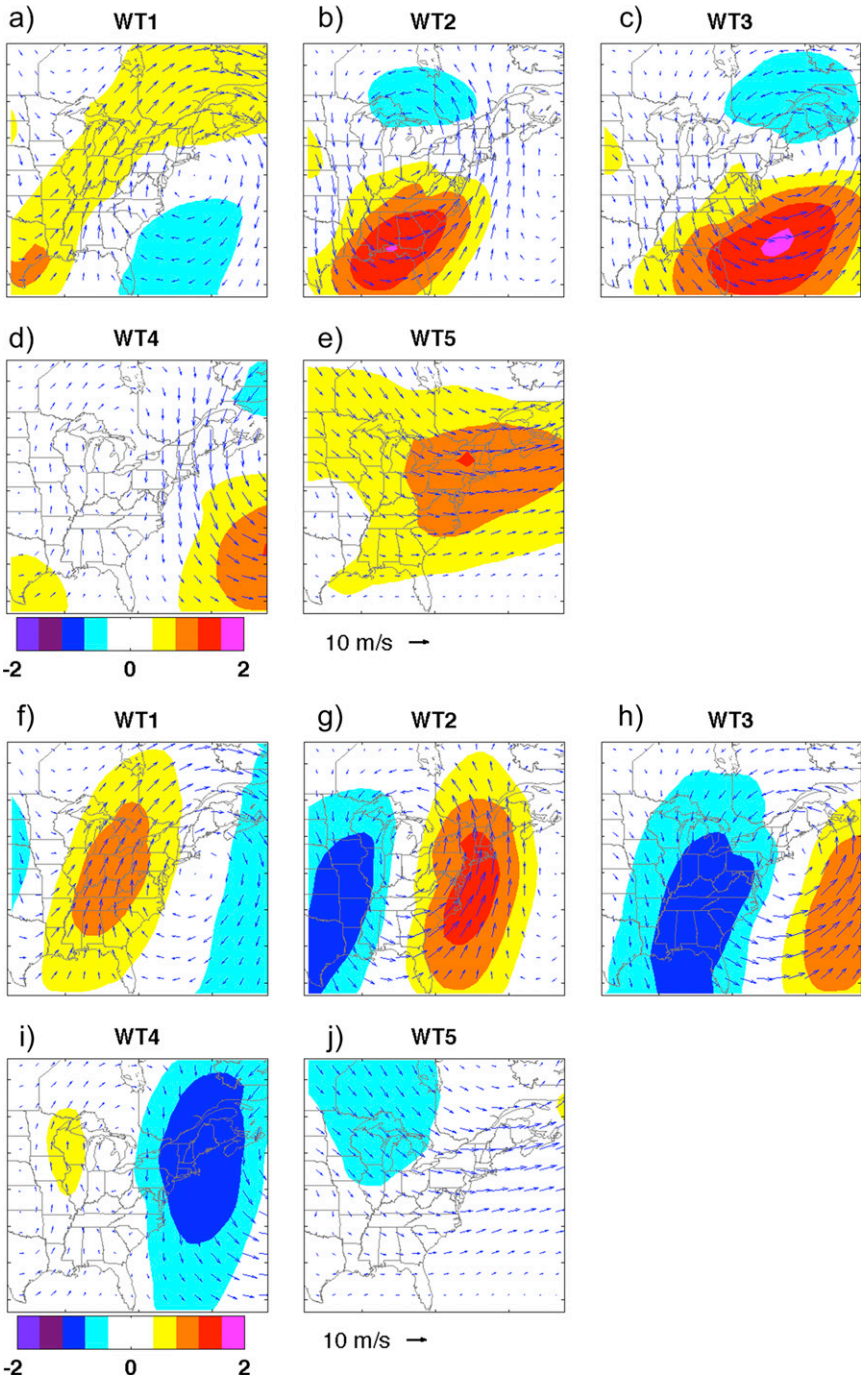

FIG. 5. MERRA 850-hPa wind anomalies (vectors) and *u*-wind standard deviations (shaded) for DJF 1981–2010 for (a) WT1, (b) WT2, (c) WT3, (d) WT4, and (e) WT5. MERRA 850-hPa wind anomalies (vectors) and *v*-wind standard deviations (shaded) for DJF 1981–2010 for (f) WT1, (g) WT2, (h) WT3, (i) WT4, and (j) WT5.

anomalously high precipitation offshore. The anomalously strong northerly flow inland indicates cold air flowing into the region, which combined with the moisture advection can indicate a strong winter storm. However, WT3 has negatively anomalous precipitation amounts all along the East Coast, indicating that this pattern likely represents 850-hPa low pressure systems outside of the "benchmark" (40°N, 70°W), which is

often used by forecasters as an important location for the track of Northeast snowstorms. In WT4, a high pressure system north of the Great Lakes allows for anomalously strong cold air advection, with little moisture, over the Northeast. WT5 has anomalously low precipitation across the entire eastern United States as a result of the strong westerly low-level jet. The cooling and drying northwesterly flow into the northern plains may set the stage for a cold front moving through the Northeast.

The reproducibility and robustness of these five WTs and how well they represent the three-dimensional circulation in the Northeast is a key question. We have assessed this both by varying the domain and time period used in the *k*-means results, and by considering other synoptic fields and levels.

We increased and decreased the domain by 1°N and 1°W and found no difference in our results (the five patterns remained essentially the same, with each pattern retaining over 90% of the same dates). However, when we increased the domain size by 4° to the north and 10° to the west, we found that *k*-means clustering suggests a sixth pattern that draws dates from WT1 and WT4. This pattern features a high pressure system off the Florida coast and a low pressure system to the west of the Great Lakes that forces moist southwesterly flow toward the Great Lakes (similar to WT1) but results in northwesterly flow over the Northeast (similar to WT4). Not surprisingly, increasing the domain size results in more complex solutions. Here, we have chosen to retain the original domain and the associated set of five patterns, since our primary goal is to explore WTs for the Northeast, and there is strong robustness for minor changes in domain size. The temporal dependence of the *k*-means solution was tested by randomly choosing 75% of the daily data before recalculating the WTs. We found that the final WTs do not change appreciably when the time period is changed.

We have also investigated using other MERRA fields for the typing analysis, since circulation at a single level may not capture the full spectrum of synoptic- and larger-scale dynamics for this region. We individually ran *k*-means clustering using 500-hPa geopotential heights and using MSLP. The former resulted in a trivial two-pattern solution of a Northeast trough in WT1 and a Northeast ridge in the other WT2, while the latter five-pattern solution was very similar to that for 850-hPa winds (but without a significant CI). We also ran a multivariate *k*-means clustering using 500-hPa geopotential heights, MSLP, and 850-hPa winds—for this the five-pattern solution was also very similar to that for the 850-hPa winds alone, but without a significant CI value. A six-pattern solution suggested by CI significance is similar to our solution using a much larger domain; however, the other objective measures for optimum *k* suggested only three or four patterns. We chose to continue to use 850-hPa winds as they produced the most robust (all objective measures of *k* in agreement) and statistically most significant classification of the winter weather types in the northeastern United States.

Another important question for a *k*-means solution is how similar each day assigned to a cluster is to the cluster centroid, since the essence of the *k*-means clustering is to maximize the intertype differences but minimize difference within each WT. We performed correlation and covariance calculations for the individual *u*- and *v*-wind components to each WT, and found that WT1 and WT3 are well correlated with both wind components, while WT4 is well correlated with the *v*-wind component. WT2 and WT5 are the least correlated. For WT5, this is not surprising since it encompasses the largest number of dates, and likely includes many patterns that are not immediately identifiable as being associated with distinct synoptic circulations.

b. *WT progression and persistence*

In addition to identifying WTs, it is useful to understand how often a particular WT transitions to each of the other WTs (Coleman and Rogers 2007b). We define ''progression'' as the percentage of time that a particular WT transitions on the following day to a different WT and ''persistence'' as the percentage of time that a particular WT remains on the following day in the same WT. Figure 6 shows the progression and persistence of each WT. The 95% confidence interval of the WT distribution on following days is determined by randomly sampling a number of days in the 30-yr record equal to each WT count, calculating the distribution of the following day WTs for each sample, and repeating the process 1000 times. The percentages that are higher (lower) than the top 97.5% (bottom 2.5%) indicate a transition to a weather type that is more (less) likely than that due to chance, and is shown as green (yellow) bars. Figure 7 shows the likelihood (expressed as percent of times) that a WT persists or transitions. WT1 is most likely to persist as WT1 or progress to WT2; WT2 is most likely to progress to WT3; WT3 is most likely to persist as WT3 or progress to WT4; and WT4 is most likely to persist as WT4 or progress to WT1. WT5 shows a high propensity for recurrence (nearly 40% of the time) but can also progress to WT1 (25% of the time). Although not significant, WT1 and WT2 may also progress to WT5. WT3 and WT4 rarely progress to WT5.

Although WTs do persist, they generally do not persist in the same weather pattern for long. The duration

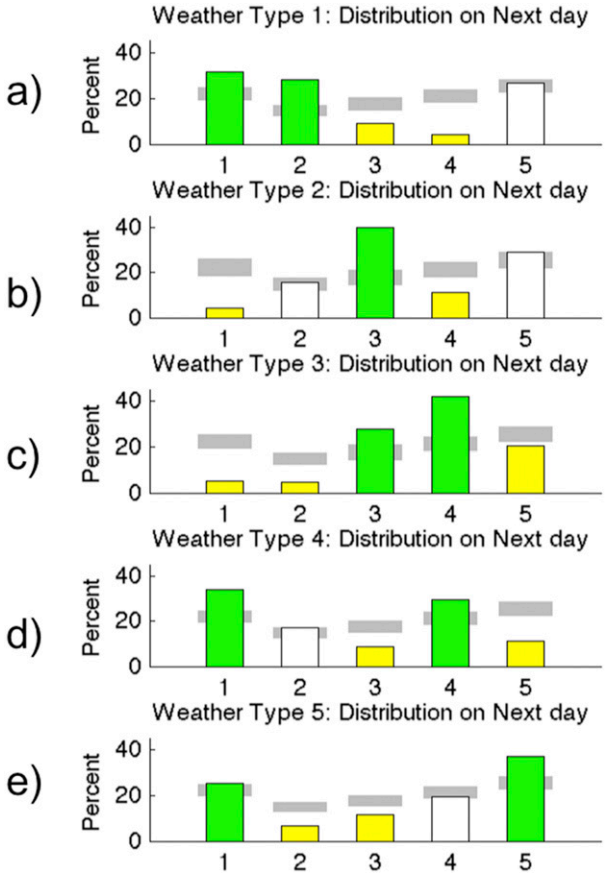

FIG. 6. Progression and persistence of each WT, shown as frequency of WTs on days following (a) WT1, (b) WT2, (c) WT3, (d) WT4, and (e) WT5 days. The 95% confidence interval of the distribution of all WTs (background frequency) is shown with gray shading. Frequencies significantly greater than the background frequency are shown as green bars; frequencies significantly less than the background frequency are shown with yellow bars (indicating a ''preferred'' progression or persistence that is likely not due to chance).

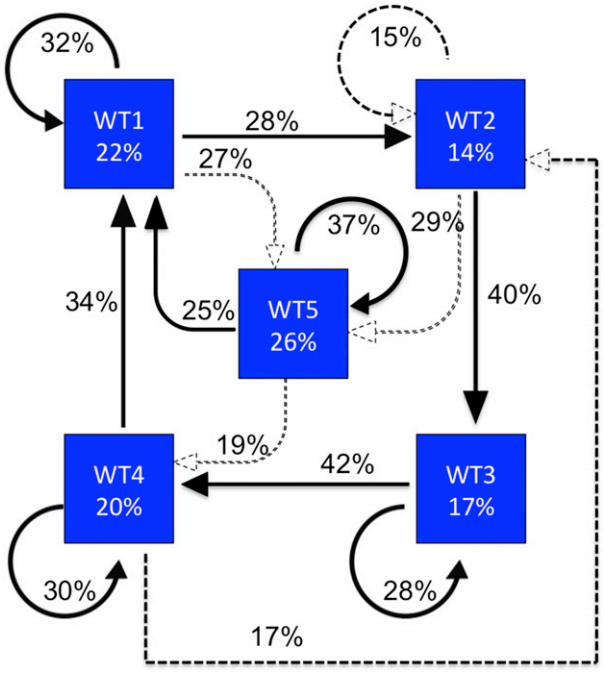

FIG. 7. Graphical representation of WT progression and persistence. The solid arrows indicate transition frequencies that are significantly higher than the background frequency (indicating a ''preferred'' progression or persistence that is likely not due to chance). Dashed arrows indicate transition frequencies that are not significantly different from the background frequency. Transitions that occur less frequently than that due to chance are not shown. The number atop each arrow indicates the percent of times the transition occurs. The background frequency of each WT is indicated in the blue squares.

for each WT is shown in Fig. 8. Only 15%–35% of DJF days persist in the same WT for 2 or more days. Only 5% of DJF days persist in the same WT for 3 or more days. The mean duration for each WT ranges from 1.17 days for WT2 to 1.58 days for WT5, and there is very little seasonal variation in duration. Consecutive WT5 days may be due to an 850-hPa low pressure system in southeastern Canada that is associated with a strong low-level jet that brings cold northwesterly air into the United States and results in a stalled low pressure system. Consecutive WT1 days may be due to a stalled high pressure system/ridge near the region, similar to a Bermuda high, that allows warm air to enter the region from the southeastern United States. The quick progression from WT2 to WT4 likely reflects troughs moving from the southeastern United States to southeast of New Brunswick.

c. *Precipitation*

To further characterize the precipitation associated with the WTs, daily precipitation and extreme precipitation are examined using station data. Daily precipitation data from 35 USHCN stations are used to calculate the number of days of precipitation (precipitation over 0.254 mm, or 0.01 in.), daily intensity on precipitation days, and total precipitation as in Agel et al. (2015). Total precipitation depends on both precipitation days and intensity. Extreme precipitation (defined as the top 1% of daily intensity on days with precipitation) is also evaluated at each station and the mean number of days of extreme precipitation, daily intensity on extreme precipitation days, and total extreme precipitation for each WT are calculated. The DJF means are shown in Table 1. Based on the station data, most precipitation days occur in WTs 2, 3, and 5. The intensity of precipitation is highest in WT2,

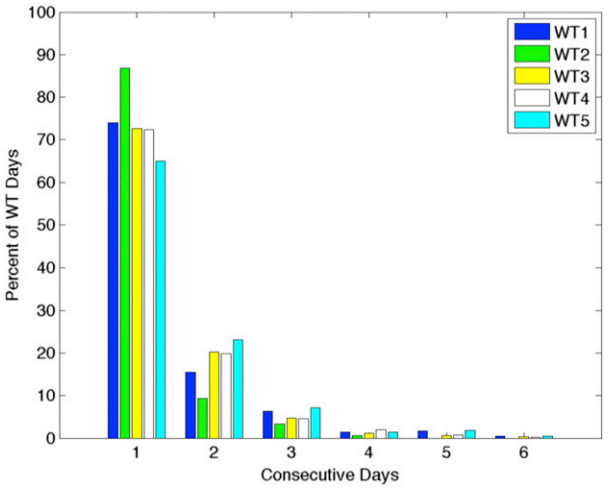

FIG. 8. WT persistence, expressed as a percent of total WT days, for durations of 1–6 days.

followed by WT3. Most extreme precipitation occurs in WT2 and WT3, with no extreme precipitation associated with WT4 and very few extreme precipitation days assigned to WT1 and WT5. Extreme precipitation intensity is also highest in WT2 and WT3. From the table it is clear that the number of precipitation days and precipitation intensity differ between WTs, but what is not clear from the table is whether precipitation is more or less likely to occur in any particular WT (i.e., if the relative frequency of precipitation days differs from the ''background frequency'' of WTs).

We use a Monte Carlo technique to determine whether station precipitation days, intensity, and totals for each WT are different than would be expected by that due to chance (the background frequency of the WTs). The WTs are randomly shuffled among the DJF days, preserving the inherent WT frequency, and the precipitation results are recalculated. This process is repeated 1000 times, providing a range of results due to chance. The results are shown in Fig. 9. Gray bars represent the 95% confidence interval of random WT assignment, while green (yellow) bars represent precipitation days, intensity, and totals more (less) likely due to chance.

Figure 9 shows that although precipitation can occur in any WT, precipitation is more likely to occur during WT2 and WT3 days (which are associated with synoptic storm features) and less likely to occur during WT1 and WT4 days (which are associated with ridges of high pressure over the Northeast or Midwest) than would be expected due to chance. These results are consistent with the gridded precipitation anomalies shown in Fig. 4. The majority of extreme precipitation days occur in WT2.

d. *Storm tracks*

Because synoptic storm features appear to play a large role in defining the WTs, it is useful to look at storm tracks for each WT. The storm-track density for each WT is plotted in Fig. 10, where the density is the cumulative count of 6-hourly storm center locations for days assigned to each WT. WT2 shows high storm-track density over the Great Lakes and Ohio Valley region with another weaker area along a coastal track. This storm track through the Great Lakes and Ohio Valley region coupled with the highly positive low-level meridional wind anomalies over the east shows that the strongest low-level wind anomalies occur in the warm sector of low pressure systems, as Booth et al. (2015) have also noted. WT3 shows a high density of coastal tracks similar to a nor'easter path. The track locations are consistent with the trough locations in Fig. 3. WT1 and WT4 show little storm activity over the Northeast, which is consistent with the ridging in Fig. 3. WT3 has high storm-track density both outside and inside of the 40°N, 70°W benchmark. When storms take a track outside of the benchmark, the precipitation shield usually does not reach New England, as cold and drier air pushes into the region from the northwest behind the low pressure system (a cold air outbreak). On the other hand, when storm tracks are closer to the coast, it allows precipitation and moisture to move inland and the cold air mixes with precipitation to create snow or at least

TABLE 1. Mean precipitation characteristics at 35 USHCN stations for DJF 1981–2010.

Category	WT1	WT2	WT3	WT4	WT5
WT days	19.8	13.0	15.6	18.8	22.8
Precipitation days	5.8	8.9	8.9	4.4	9.3
Probability of precipitation (%)	29.3	68.5	57.1	23.4	40.8
Precipitation intensity (mm day^{-1})	4.3	10.4	6.5	2.8	4.3
Precipitation total (mm)	24.8	93.1	57.8	12.1	40.0
Extreme precipitation days	0.006	0.071	0.034	0.000	0.004
Extreme precipitation intensity (mm day^{-1})	40.9	57.0	65.4	—	45.1
Extreme precipitation total (mm)	0.25	4.07	2.2	—	0.18

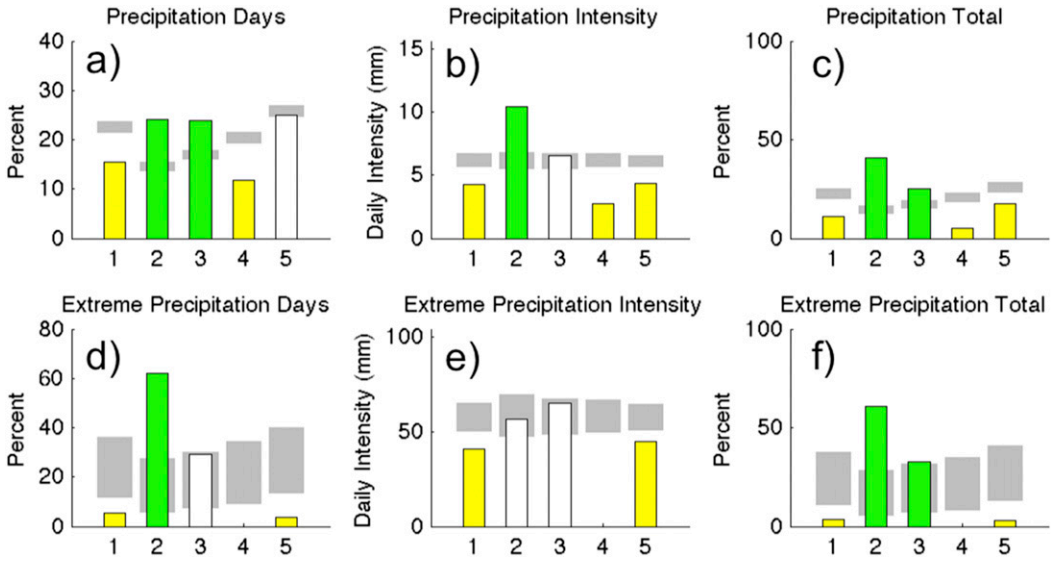

FIG. 9. Station precipitation characteristics of the WTs. (a) The number of precipitation days (expressed as a percent of all precipitation days) for each WT. The frequency is a mean of station precipitation days. The 95% confidence interval of the background frequency is shown with gray shading. Frequencies significantly greater than the background frequency are shown as green bars; frequencies significantly less than the background frequency are shown as yellow bars (indicating a distribution that is likely not due to chance). (b) The mean daily precipitation intensity (mm day^{-1}) for each WT. (c) The mean total precipitation (%) for each WT. The 95% confidence interval of precipitation intensity and total precipitation (gray shading) indicates the intensity range given random distribution of the WTs. (d)–(f) Precipitation days, intensity, and totals for extreme precipitation, defined as the top 1% of precipitation daily intensity. Precipitation data from 35 USHCN stations for DJF 1981–2010.

more wintry precipitation. WT5 has light storm-track density in the Northeast with higher density in far northern New England and eastern Canada. Since WT5 has a moderate number of precipitation days and relatively low precipitation intensity, this may indicate that precipitation in this WT is related to lake-effect snow, as well as general instability due to shortwave activity associated with the northern low.

Storm tracks on extreme precipitation days within each WT are also considered (Fig. 11). To be considered an extreme precipitation day, at least one station on that day must experience precipitation in the top 1% of wet days in the 30-yr station record. The vast majority of extreme precipitation days occurs in WT2 and WT3; not surprisingly, these are associated with high densities of storm tracks. As with all precipitation days, extreme precipitation in WT2 appears to be related to storms near the Great Lakes region as well as coastal storms, while extreme precipitation in WT3 appears to be related to coastal storm paths.

e. Teleconnections

Our analysis for the teleconnections was performed by taking the daily phase of NAO, PNA, and AO, and the monthly phase of ENSO, as well as the WT assigned to each day, and determining the relative frequency of WTs for each teleconnection phase. In Fig. 12, the percent occurrence of the WTs during positive, neutral, and negative phases is compared to the WT "background" frequency. The WT background frequency used for NAO, PNA, and AO results is calculated using a Monte Carlo technique, in which WTs are randomly shuffled among the DJF days, preserving the inherent WT frequency, and the WT frequency during positive, neutral, and negative days is calculated using the randomized data. The process is repeated 1000 times, providing a range of background frequency distributions of the WTs for each teleconnection phase. Departures outside the 95% confidence interval of the background frequency are shaded green for positive results (more likely to occur than by chance) and yellow for negative results (less likely to occur than by chance).

During the positive phase of the NAO (NAO $>$ 1), the likelihood of WT1 increases while the likelihood of WT2, WT3, and WT4 decreases. During the neutral phase of the NAO ($-1 \leq$ NAO ≤ 1), the likelihood of WT1 decreases slightly, while the likelihood of WT2 increases slightly. During the negative phase of the NAO (NAO < -1), the likelihood of WT1 decreases, while the likelihood of WT4 increases. WT5 has no statistically significant changes in frequency for any phase of the NAO. NAO has the strongest link to WT1

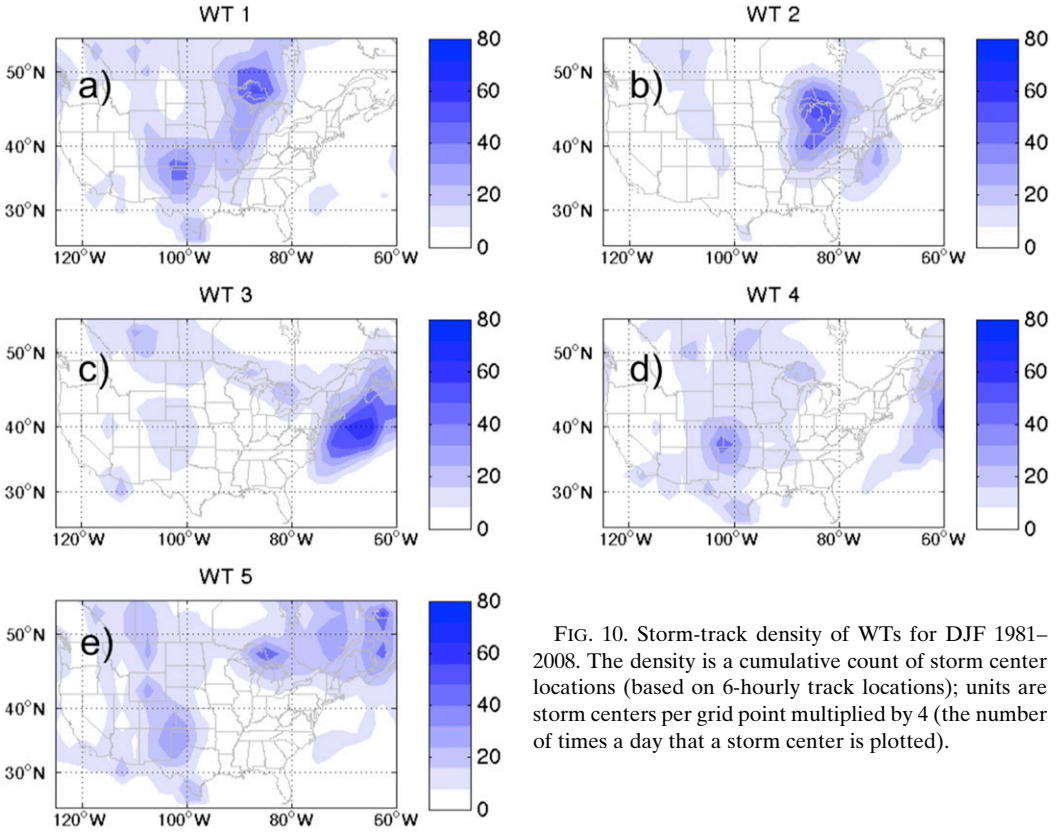

FIG. 10. Storm-track density of WTs for DJF 1981–2008. The density is a cumulative count of storm center locations (based on 6-hourly track locations); units are storm centers per grid point multiplied by 4 (the number of times a day that a storm center is plotted).

and WT4, resulting in a twofold difference in frequency of days depending on phase. This link may be related to the warm southerly flow in WT1 versus the cooler northerly flow in WT4 because the positive (negative) NAO has warmer (cooler) surface temperatures in the eastern United States. For WT4, the strong northerly flow brings cooler temperatures over the East Coast, which occurs more often in the negative phase of the NAO.

During the positive phase of the AO (AO > 1), the likelihood of WT1 and WT5 increases while the likelihood of WT3 and WT4 decreases. During the neutral phase of the AO ($-1 \leq$ AO ≤ 1), the likelihood of WT1 increases while the likelihood of WT5 slightly decreases. During the negative AO phase (AO < -1), the likelihood of WT3 and WT4 increases while the likelihood of WT1 and WT5 decreases (opposite for positive AO, although the result for WT5 is not statistically significant). WT2 has no statistically significant changes in frequency for any phase of the AO. Like the NAO, the AO phase nearly doubles or halves the frequency of WT1 and WT4.

During the positive phase of the PNA (PNA > 1), the likelihood of WT1 decreases, while the likelihood of WT3 increases. During the neutral phase of the PNA ($-1 \leq$ PNA ≤ 1), the likelihood of WT3 slightly decreases. During the negative phase of the PNA (PNA < -1), the likelihood of WT1 increases while the likelihood of WT3 decreases (opposite for positive PNA). There are no statistically significant deviations from background frequency for WT2, WT4, and WT5 during any phase of PNA. The PNA has the strongest link to WT1 and WT3, resulting in a twofold difference in frequency of days depending on phase. The positive PNA phase may be reflected in WT3 by the strong storm and cool temperatures along the East Coast, whereas the negative PNA phase may be reflected in WT1 by the warm temperatures and high pressure along the East Coast. In addition, the meridional flow anomalies hint at wave patterns in both of those WTs.

During the warm phase of ENSO (Niño-3.4 > 1), the likelihood of WT3 increases, while the likelihood of WT5 decreases. During the cold phase of ENSO (Niño-3.4 < -1), the likelihood of WT3 slightly decreases. No statistically significant deviations from WT background frequencies are evident for the neutral phase of ENSO. For all the preceding results, it should be noted that while we have defined positive and negative phases of various teleconnections as greater than or less than 1,

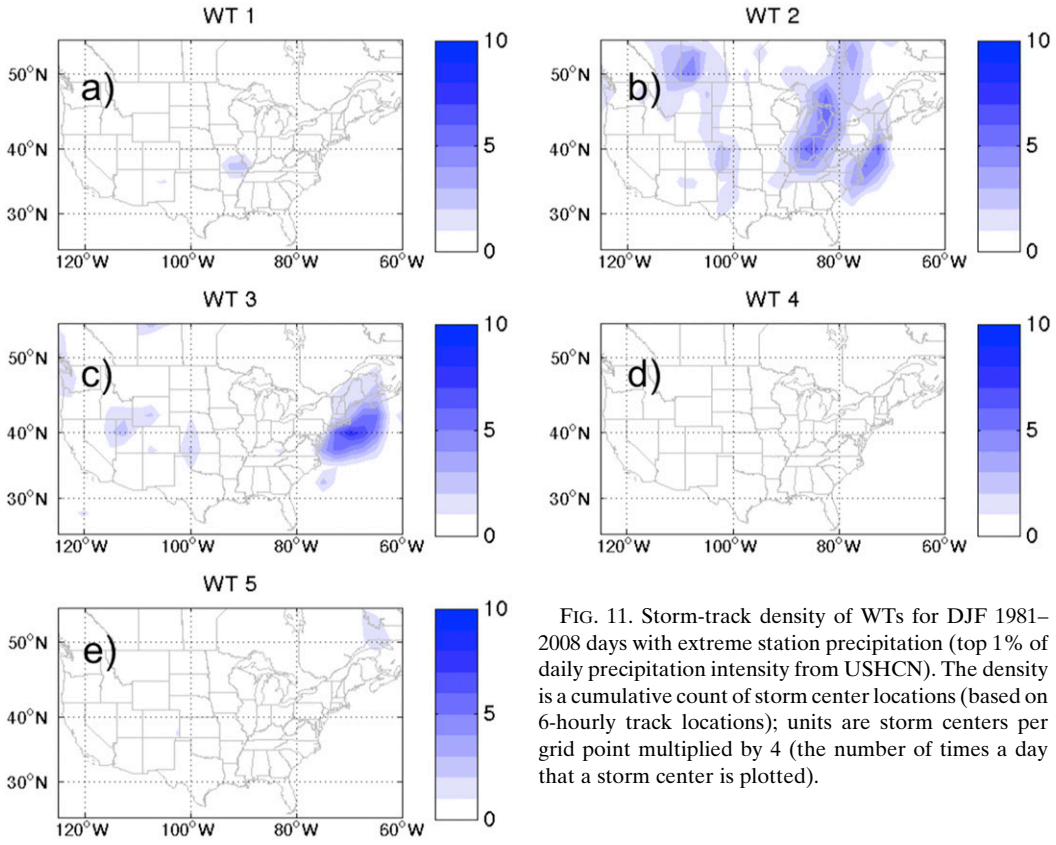

FIG. 11. Storm-track density of WTs for DJF 1981–2008 days with extreme station precipitation (top 1% of daily precipitation intensity from USHCN). The density is a cumulative count of storm center locations (based on 6-hourly track locations); units are storm centers per grid point multiplied by 4 (the number of times a day that a storm center is plotted).

our results are also statistically robust for defining phases as greater than or less than 0.5.

4. Summary and discussion

In this study, we apply *k*-means cluster analysis to wintertime daily 850-hPa winds in the Northeast using MERRA data from 1981 to 2010. Using this technique, five distinct WTs are identified. Each WT is considered in terms of mean and anomalous 850-hPa winds and gridded precipitation, and the transitioning and persistence of each WT are analyzed. Each WT is then examined for links to station precipitation and extreme precipitation, storm tracks, and teleconnections.

WT1 is characterized by a ridge just off the U.S. East Coast and positive precipitation anomalies as far north as the Great Lakes. A second pattern (WT2) features a trough along the eastern United States and positive precipitation anomalies into southern New England. In the third pattern (WT3), a trough resides over the western Atlantic and negative precipitation anomalies occur along much of the U.S. East Coast. WT4 is characterized by a trough east of Newfoundland and negative precipitation anomalies along parts of the U.S. East Coast. The fifth and final pattern (WT5) features a broad, shallow trough over southeastern Canada and negative precipitation anomalies over the entire U.S. East Coast. The relative frequency of each WT ranges from ~15% to 25% of the DJF days, with WT2 (14%) having the least number of days, and WT5 (26%) having the greatest number of days.

Anomalously negative zonal winds (strong easterlies) at 850 hPa have been associated with heavy rainfall and East Coast winter storms (Stuart and Grumm 2006). WT3 shows the strongest negative zonal wind anomalies over the Northeast. Although not the 3–5 standard deviations below normal that Stuart and Grumm (2006) found for their case studies, the strongly anomalous easterly winds in WT3 do nevertheless suggest strong winter storms (one possible reason for our smaller standard deviations could be compositing). However, the lack of precipitation over the region may be the result of a mix of the storm itself passing just outside of the 40°N, 70°W benchmark and dry northwesterly air cutting off precipitation.

In terms of transitioning from one WT to another, WT1 (ridging in the Northeast) tends to persist or transition to WT5 (zonal flow) or WT2 (eastern United

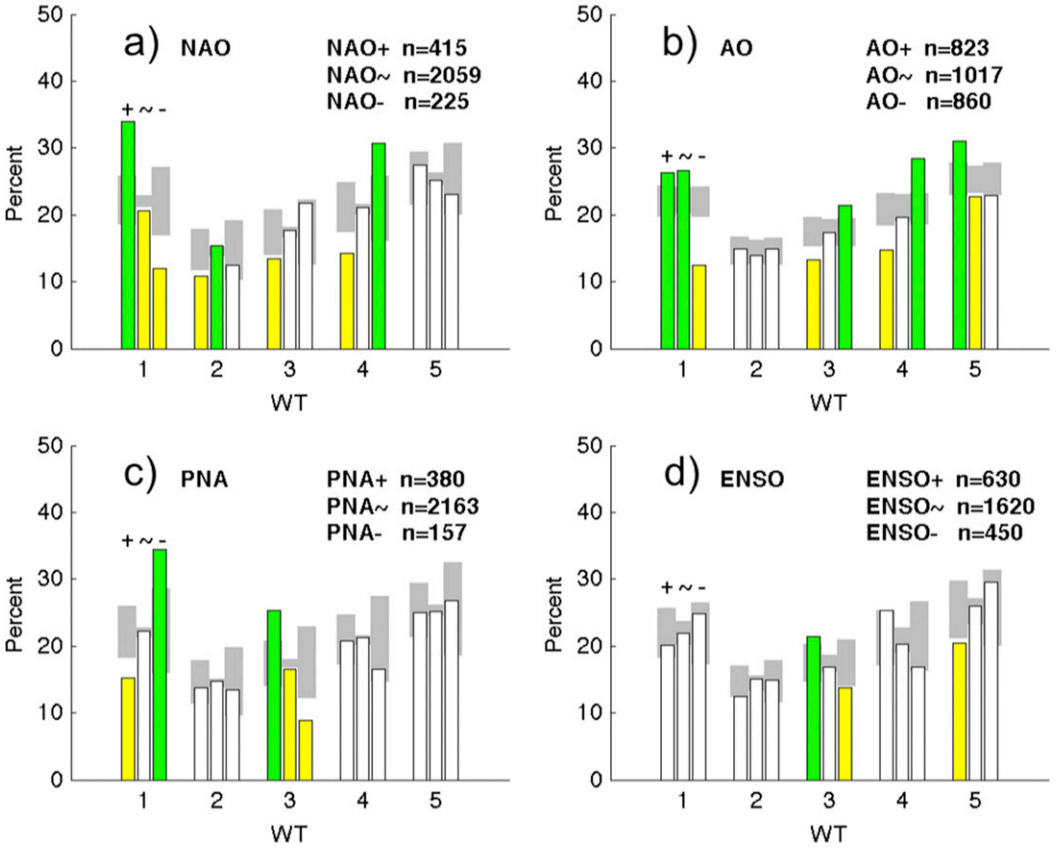

FIG. 12. WT frequency during various phases of (a) NAO, (b) AO, (c) PNA, and (d) ENSO. For each WT, the three bars represent the positive, neutral, and negative phases of the teleconnection pattern. The 95% confidence interval of the WT background frequency (the distribution of WTs in each phase due to chance) is shown with gray shading. Frequencies significantly greater than the background frequency are shown as green bars; frequencies significantly less than the background frequency are shown with yellow bars (indicating a distribution that is likely not due to chance). The number of positive, neutral, and negative phases for each index is indicated.

States trough). WT2 tends to transition to WT3 (coastal trough), which then tends to persist or transition to WT4 (western Atlantic trough). WT5 is the most persistent pattern, possibly due to a cutoff upper-level low over Canada. WT5 is also likely to transition to WT1. While the progression from WT1 to WT2 to WT3 to WT4 and then back to WT1 could be considered a typical synoptic storm path through the region, WT1 is actually more likely to persist than transition to WT2. However, once the transition to WT2 occurs, WT2 quickly transitions to WT3, consistent with the movement of wintertime synoptic storms. Figure 13 summarizes these results by combining the large-scale and anomalous flow from Figs. 3 and 4 and the favored transitions of the WTs from Fig. 7. Overall, an eastward movement of the trough can be observed along with a phase transition from −PNA to +PNA and +NAO to −NAO. When considering the longevity of our WTs, other studies have shown regimes that last for a longer period of time (e.g., Archambault et al. 2010), whereas our WTs typically change on a time scale of 1–3 days. This may arise because we have derived the WTs from the lower-level 850-hPa winds in a smaller region.

Teleconnections also can play a role in wintertime weather over the northeastern United States. To understand that role, the frequency of each WT during the various phases of the NAO, AO, PNA, and ENSO are evaluated. WT1, with northwesterly flow and little precipitation, is more likely to occur during the positive phase of the NAO, the neutral or positive phase of the AO, and the negative phase of the PNA. WT2 (eastern U.S. trough) is more likely to occur during the neutral phase of the NAO. WT3 and WT4 (troughs located just offshore or farther to the east over the Atlantic) are more likely to occur during the negative phase of the AO. In addition, WT3 is more likely to occur during the positive phase of the PNA, while WT4 is more likely to occur during the negative phase of the NAO. WT5, with

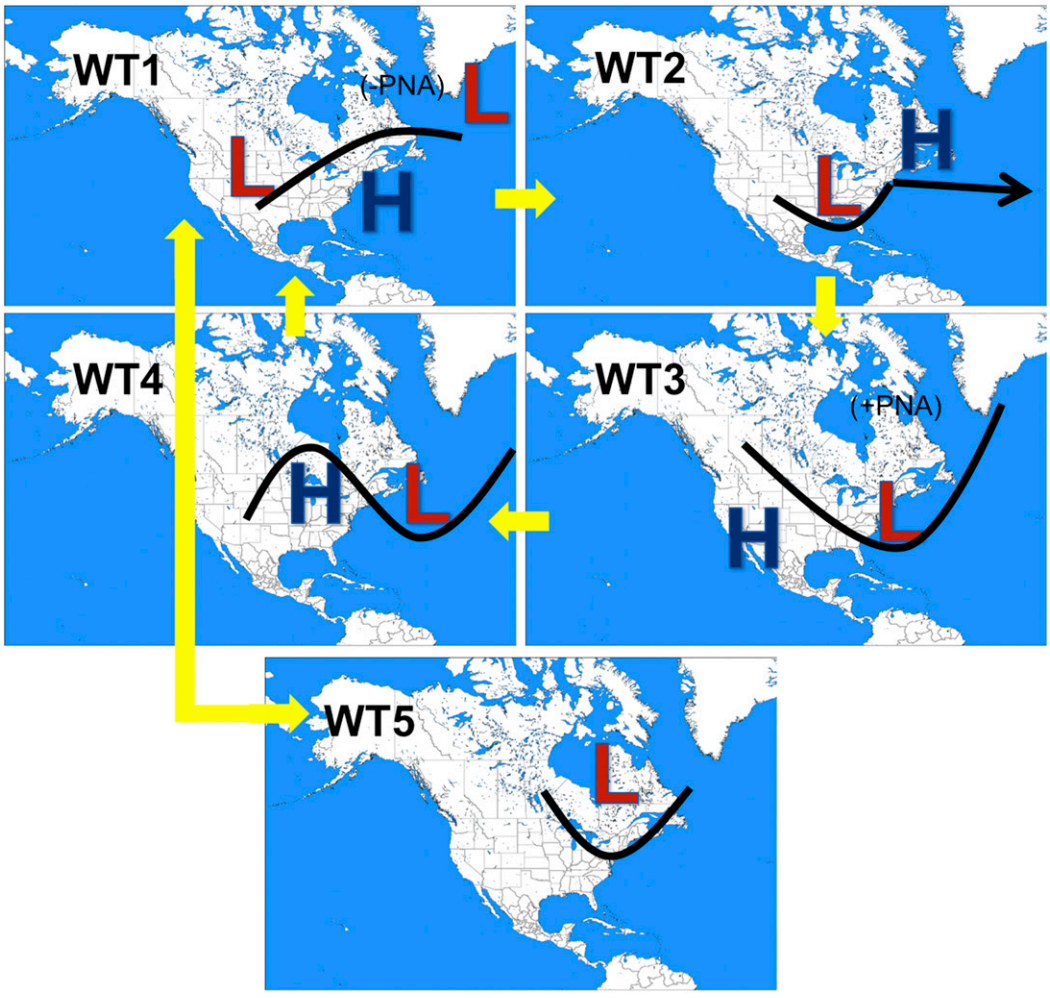

FIG. 13. Summary of WT characteristics from *k*-means clustering: WT1: coastal ridge type; WT2: coastal land trough type; WT3: coastal ocean trough type; WT4: Mid–Atlantic Ocean trough type; and WT5: zonal flow type. Each panel shows the dominant large-scale circulation, areas of anomalous low and high pressure, and preferred transitions to other WTs.

zonal flow and light precipitation, is more likely to occur during the positive phase of the AO. ENSO shows little effect on the WTs, except for WT3, which is more likely to occur during the warm phase of ENSO. Overall, NAO has a strong link to WT1 and WT4, which tend to be low-precipitation patterns in the Northeast. PNA has a strong link to WT1 (low precipitation) and WT3 (nonextreme precipitation). It also appears that the PNA, NAO, and AO all have closer links to the WTs as a whole than ENSO does, which echoes previous research (Huntington et al. 2004).

Bradbury et al. (2002) and Notaro et al. (2006) noted that the PNA helped to identify the meridional waviness of a pattern, but disagreed on how much impact the PNA had on the overall pattern as a result of not being able to completely resolve the east–west shift of the East Coast pressure trough (Bradbury et al. 2002). However, Notaro et al. (2006) did show that the PNA is associated with a slight southeastward shift of the jet stream and, as a result, the storm track. This shift in storm track can be seen in the storm-track composites (Fig. 10). WT1, which may occur more often in negative PNA phase patterns, has a storm track more northwestward than that of WT3, which may occur more often in positive PNA phase patterns. We can also consider the singular and combined influence of the teleconnections by performing logistic regression using the indices as predictors of the occurrence of the WTs. Calculation of the cross-validated deviance from the regression results confirms that ENSO has little overall influence over the WTs, while AO shows the greatest influence, followed closely by NAO and PNA, and the combined NAO/PNA

TABLE 2. WTs with a statistically significant increase in likelihood during positive (+), negative (−), and neutral (~) phases of various teleconnections. Also shown are correlations with above-normal (↑) or below-normal precipitation (↓) as contributed from each WT, along with areas of placement of highest storm-track density.

WT	NAO	AO	PNA	ENSO	Precipitation	Storm track
WT1	+	+ ~	−		↓	
WT2	~				↑	Great Lakes, coastal
WT3	−	−	+	+	↑	Coastal
WT4	−	−			↓	
WT5		+				

has greater skill than any single teleconnection or any other combination of two teleconnections at predicting daily WTs, particularly for WT1 and WT3.

Table 2 summarizes each of these results, showing the links to the various teleconnection phases, the correlation to higher or lower amounts of precipitation, and the location of storm tracks for each WT. Note that the precipitation variation in the table is only the contribution from that WT, not the variation of total seasonal precipitation (which is the combined contribution of all WTs). Although each of these teleconnection patterns can be considered separately, we may gain more insight by considering their features together and looking at phase transitions. In Archambault et al. (2010), it was demonstrated that precipitation occurs more often during a 6-month period of November–April in the northeastern United States, with an evolution from a more zonal to amplified wavy flow. Similarly, in this study, we find transitions from WT1 to WT4 may be associated with a shift from positive NAO to negative NAO, and consequently from more zonal to more amplified flow, and an associated increase in precipitation in WT2. Both Notaro et al. (2006), whose study considered only December, and Archambault et al. (2010) found that positive PNA and negative NAO coupled together create the least amount of precipitation, and that a negative PNA coupled with a positive NAO created the greatest amount of precipitation. Their results, however, differ from ours (in which the December–February period is considered) for the Northeast in terms of precipitation. In those studies, different time periods and different geographical locations (we do not include stations in Pennsylvania, for example) were used to calculate the averaged total precipitation. Therefore, the discrepancy may come from spatial heterogeneity and subseasonal variability of the underlying data. The spatial heterogeneity in precipitation anomalies in the northeastern United States is evident in WT1 and WT3 (Fig. 4). For example, WT1 has greater chance of occurrence in −PNA/+NAO, but the precipitation pattern shows opposite signs of anomalies between the western and eastern part of the domain (Fig. 4a). Therefore, different areas used for averaging precipitation may produce opposite signs of results in precipitation anomalies. If we focus on other related aspects of the WTs, our results are consistent with the previous studies. For instance, more coastal storms (WT3) occur during +PNA/−NAO phases.

When we compare our WTs to Ning and Bradley (2014), who proposed three EOFs to describe the variability of wintertime (December–March) precipitation anomalies, the closest match is our WT3 to their EOF3 in terms of teleconnections. However, their respective precipitation anomalies are quite different with EOF3 having above-normal precipitation anomalies along the East Coast and WT3 having below-normal precipitation anomalies in the same location. A reason for this could be because of the extra influence of the positive Pacific decadal oscillation (PDO) in EOF3, which increases precipitation totals and is not considered in our study, as well as our differing definitions of wintertime. However, we do show a slight increase in station precipitation (especially along the immediate coast) in WT3, consistent with their results. The negative anomalies for the overall region may be related to enhanced stability and subsidence along the East Coast combined with lower moisture content (Notaro et al. 2006), especially since WT3 may be more likely with positive PNA.

Comparison of our results with previous studies (Notaro et al. 2006; Archambault et al. 2008, 2010) indicates that the impact of large-scale teleconnection patterns on regional climate in the northeastern United States is not spatially homogeneous. These results also show that analyses carried out for different time periods can produce different results, indicating subseasonal variability of the WTs. This kind of subseasonal variability of the WTs, as well as spatial heterogeneity of precipitation anomalies, warrants further investigation.

Acknowledgments. This work was supported by the NASA National Climate Assessment Grant NNX13AN36G and NSF Grant 0811099. Constructive comments from three anonymous reviewers were helpful for improving the paper.

REFERENCES

Agel, L., M. Barlow, J. Qian, F. Colby, E. Douglas, and T. Eichler, 2015: Climatology of daily precipitation and extreme precipitation events in the northeast United States. *J. Hydrometeor.*, **16**, 2537–2557, doi:10.1175/JHM-D-14-0147.1.

Archambault, H. M., L. F. Bosart, D. Keyser, and A. R. Aiyyer, 2008: Influence of large-scale flow regime on cool-season

precipitation in the northeastern United States. *Mon. Wea. Rev.*, **136**, 2945–2963, doi:10.1175/2007MWR2308.1.

——, D. Keyser, and L. F. Bosart, 2010: Relationships between large-scale regime transitions and major cool-season precipitation events in the northeastern United States. *Mon. Wea. Rev.*, **138**, 3454–3473, doi:10.1175/2010MWR3362.1.

Armstrong, R. L., and M. J. Brodzik, 1995: An Earth-gridded SSM/I data set for cryospheric studies and global change monitoring. *Adv. Space Res.*, **16**, 155–163, doi:10.1016/0273-1177(95)00397-W.

Ashouri, H., K.-L. Hsu, S. Sorooshian, D. K. Braithwaite, K. R. Knapp, L. D. Cecil, B. R. Nelson, and O. P. Prat, 2015: PERSIANN-CDR: Daily precipitation climate data record from multisatellite observations for hydrological and climate studies. *Bull. Amer. Meteor. Soc.*, **96**, 69–83, doi:10.1175/BAMS-D-13-00068.1.

Bai, X., J. Wang, C. Sellinger, A. Clites, and R. Assel, 2010: The impacts of ENSO and AO/NAO on the interannual variability of Great Lakes ice cover. NOAA Tech. Memo. GLERL 152, 44 pp.

Barnston, A. G., and R. E. Livezey, 1987: Classification, seasonality, and persistence of low-frequency atmospheric circulation patterns. *Mon. Wea. Rev.*, **115**, 1083–1126, doi:10.1175/1520-0493(1987)115<1083:CSAPOL>2.0.CO;2.

Boé, J., and L. Terray, 2008: A weather-type approach to analyzing winter precipitation in France: Twentieth-century trends and the role of anthropogenic forcing. *J. Climate*, **21**, 3118–3133, doi:10.1175/2007JCLI1796.1.

Booth, J. F., H. Reider, D. E. Lee, and Y. Kushnir, 2015: The paths of extratropical cyclones associated with wintertime high-wind events in the northeastern United States. *J. Appl. Meteor. Climatol.*, **54**, 1871–1885, doi:10.1175/JAMC-D-14-0320.1.

Bradbury, J. A., B. D. Keim, and C. P. Wake, 2002: U.S. East Coast trough indices at 500 hPa and New England winter climate variability. *J. Climate*, **15**, 3509–3517, doi:10.1175/1520-0442(2002)015<3509:USECTI>2.0.CO;2.

——, ——, and ——, 2003: The influence of regional storm tracking and teleconnections on winter precipitation in the northeastern United States. *Ann. Assoc. Amer. Geogr.*, **93**, 544–556, doi:10.1111/1467-8306.9303002.

Coleman, J. S. M., and J. C. Rogers, 2007a: A synoptic climatology of the central United States and associations with Pacific teleconnection pattern frequency. *J. Climate*, **20**, 3485–3497, doi:10.1175/JCLI4201.1.

——, and ——, 2007b: Regional synoptic classification schemes: A Midwestern example. *Climate Variability, Predictability, and Change in the Midwest*, S. C. Pryor, Ed., Indiana University Press, 208–218.

Conway, D., and P. D. Jones, 1998: The use of weather types and air flow indices for GCM downscaling. *J. Hydrol.*, **212–213**, 348–361, doi:10.1016/S0022-1694(98)00216-9.

Demuzere, M., M. Werner, N. P. M. van Lipzig, and E. Roeckner, 2009: An analysis and future ECHAM5 pressure fields using a classification of circulation patterns. *Int. J. Climatol.*, **29**, 1796–1810, doi:10.1002/joc.1821.

Diday, E., and J. J. Simon, 1976: Clustering analysis. *Digital Pattern Recognition*, K. S. Fu, Ed., Springer, 47–94.

Easterling, D. R., T. R. Karl, J. H. Lawrimore, and S. A. Del Greco, 1999: United States Historical Climatology Network daily temperature, precipitation, and snow data for 1871–1997. ORNL/CDIAC-118, NDP-070, Carbon Dioxide Information Analysis Center, Oak Ridge National Laboratory, 84 pp.

Eichler, T., and W. Higgins, 2006: Climatology and ENSO-related variability of North American extratropical cyclone activity. *J. Climate*, **19**, 2076–2093, doi:10.1175/JCLI3725.1.

Ghil, M., and A. W. Robertson, 2002: "Waves" vs. "particles" in the atmosphere's phase space: A pathway to long-range forecasting? *Proc. Natl. Acad. Sci. USA*, **99**, 2493–2500, doi:10.1073/pnas.012580899.

Hirsch, M. E., A. T. DeGaetano, and S. J. Colucci, 2001: An East Coast winter storm climatology. *J. Climate*, **14**, 882–899, doi:10.1175/1520-0442(2001)014<0882:AECWSC>2.0.CO;2.

Huntington, T. G., G. A. Hodgkins, B. D. Keim, and R. W. Dudley, 2004: Changes in the proportion of precipitation occurring as snow in New England. *J. Climate*, **17**, 2626–2636, doi:10.1175/1520-0442(2004)017<2626:CITPOP>2.0.CO;2.

Jones, G. V., and R. E. Davis, 1995: Climatology of nor'easters and the 30 kPa jet. *J. Coast. Res.*, **11**, 1210–1220.

Kahya, E., and J. A. Dracup, 1993: U.S. streamflow patterns in relation to the El Niño/Southern Oscillation. *Water Resour. Res.*, **29**, 2491–2503, doi:10.1029/93WR00744.

Kanamitsu, M., W. Ebisuzaki, J. Woollen, S. K. Yang, J. J. Hnilo, M. Fiorino, and G. L. Potter, 2002: NCEP–DOE AMIP-II Reanalysis (R-2). *Bull. Amer. Meteor. Soc.*, **83**, 1631–1643, doi:10.1175/BAMS-83-11-1631.

Kunkel, K. E., and J. R. Angel, 1999: Relationship of ENSO to snowfall and related cyclone activity in the contiguous United States. *J. Geophys. Res.*, **104**, 19 425–19 434, doi:10.1029/1999JD900010.

Lana, X., and G. Fernandez-Mills, 1994: Minimum sample size for synoptic weather type classification. Application to winter period data recorded on the Catalan coast (northeast Spain). *Int. J. Climatol.*, **14**, 1051–1060, doi:10.1002/joc.3370140909.

Leathers, D. J., B. Yarnal, and M. A. Palecki, 1991: The Pacific/North American teleconnection pattern and United States climate. Part I: Regional temperature and precipitation associations. *J. Climate*, **4**, 517–528, doi:10.1175/1520-0442(1991)004<0517:TPATPA>2.0.CO;2.

Michelangeli, P., R. Vautard, and B. Legras, 1995: Weather regimes: Recurrence and quasi stationarity. *J. Atmos. Sci.*, **52**, 1237–1256, doi:10.1175/1520-0469(1995)052<1237:WRRAQS>2.0.CO;2.

Moron, V., A. W. Robertson, M. N. Ward, and O. Ndiaye, 2008: Weather types and rainfall over Senegal. Part I: Observational analysis. *J. Climate*, **21**, 266–287, doi:10.1175/2007JCLI1601.1.

——, ——, and J.-H. Qian, 2010: Local versus regional-scale characteristics of monsoon onset and post-onset rainfall over Indonesia. *Climate Dyn.*, **34**, 281–299, doi:10.1007/s00382-009-0547-2.

NASA, 2014: MERRA data holdings. Goddard Earth Sciences Data and Information Services Center, accessed 1 February 2014. [Available online at http://disc.sci.gsfc.nasa.gov/daac-bin/DataHoldings.pl.]

NCDC, 2015: PERSIANN data files. National Climatic Data Center, accessed 10 July 2015 [Available online at ftp://data.ncdc.noaa.gov/cdr/persiann/files/.]

Ning, L., and R. S. Bradley, 2014: Winter precipitation variability and corresponding teleconnections over the northeastern United States. *J. Geophys. Res. Atmos.*, **119**, 7931–7945, doi:10.1002/2014JD021591.

Notaro, M., W.-C. Wang, and W. Gong, 2006: Model and observational analysis of the northeast U.S. regional climate and its relationship to the PNA and NAO patterns during early winter. *Mon. Wea. Rev.*, **134**, 3479–3505, doi:10.1175/MWR3234.1.

Patten, J. M., S. R. Smith, and J. J. O'Brien, 2003: Impacts of ENSO on snowfall frequencies in the United States. *Wea. Forecasting*, **18**, 965–980, doi:10.1175/1520-0434(2003)018<0965:IOEOSF>2.0.CO;2.

Perez, J., M. Menendez, F. J. Mendez, and I. J. Losado, 2014: Evaluating the performance of CMIP3 and CMIP5 global climate models over the north-east Atlantic region. *Climate Dyn.*, **43**, 2663–2680, doi:10.1007/s00382-014-2078-8.

Piechota, T. C., and J. A. Dracup, 1996: Drought and regional hydrologic variation in the United States: Associations with El Niño–Southern Oscillation. *Water Resour. Res.*, **32**, 1359–1373, doi:10.1029/96WR00353.

Qian, J.-H., A. W. Robertson, and V. Moron, 2010: Interactions among ENSO, the monsoon, and diurnal cycle in rainfall variability over Java, Indonesia. *J. Atmos. Sci.*, **67**, 3509–3524, doi:10.1175/2010JAS3348.1.

Rasmusson, E. M., and T. H. Carpenter, 1982: Variations in tropical sea surface temperature and surface wind fields associated with the Southern Oscillation/El Niño. *Mon. Wea. Rev.*, **110**, 354–384, doi:10.1175/1520-0493(1982)110<0354:VITSST>2.0.CO;2.

Reynolds, R. W., N. A. Rayner, T. M. Smith, D. C. Stokes, and W. Wang, 2002: An improved in situ and satellite SST analysis for climate. *J. Climate*, **15**, 1609–1625, doi:10.1175/1520-0442(2002)015<1609:AIISAS>2.0.CO;2.

Riddle, E. E., M. B. Stoner, N. C. Johnson, M. L. L'Heureux, D. C. Collins, and S. B. Feldstein, 2013: The impact of the MJO on clusters of wintertime circulation anomalies over the North American region. *Climate Dyn.*, **40**, 1749–1766, doi:10.1007/s00382-012-1493-y.

Rienecker, M. M., and Coauthors, 2011: MERRA: NASA's Modern-Era Retrospective Analysis for Research and Applications. *J. Climate*, **24**, 3624–3648, doi:10.1175/JCLI-D-11-00015.1.

Rogers, J. C., 1984: The association between the North Atlantic Oscillation and the Southern Oscillation in the Northern Hemisphere. *Mon. Wea. Rev.*, **112**, 1999–2015, doi:10.1175/1520-0493(1984)112<1999:TABTNA>2.0.CO;2.

Rohli, R. V., and A. J. Vega, 2008: *Climatology*. Jones and Bartlett, 466 pp.

Ropelewski, C. F., and M. S. Halpert, 1986: North American precipitation and temperature patterns associated with the El Niño/Southern Oscillation (ENSO). *Mon. Wea. Rev.*, **114**, 2352–2362, doi:10.1175/1520-0493(1986)114<2352:NAPATP>2.0.CO;2.

——, and ——, 1987: Global and regional scale precipitation patterns associated with the El Niño/Southern Oscillation. *Mon. Wea. Rev.*, **115**, 1606–1626, doi:10.1175/1520-0493(1987)115<1606:GARSPP>2.0.CO;2.

Serreze, M. C., 1995: Climatological aspects of cyclone development and decay in the Arctic. *Atmos.–Ocean*, **33**, 1–23, doi:10.1080/07055900.1995.9649522.

——, F. Carse, R. G. Barry, and J. C. Rogers, 1997: Icelandic low cyclone activity: Climatological features, linkages with the NAO, and relationships with recent changes in the Northern Hemisphere circulation. *J. Climate*, **10**, 453–464, doi:10.1175/1520-0442(1997)010<0453:ILCACF>2.0.CO;2.

Sheridan, S. C., 2002: The redevelopment of a weather-type classification scheme for North America. *Int. J. Climatol.*, **22**, 51–68, doi:10.1002/joc.709.

Stahl, K., R. D. Moore, and I. G. Mckendry, 2006: The role of synoptic-scale circulation in the linkage between large-scale ocean–atmosphere indices and winter surface climate in British Columbia, Canada. *Int. J. Climatol.*, **26**, 541–560, doi:10.1002/joc.1268.

Straus, D. M., S. Corti, and F. Molteni, 2007: Circulation regimes: Chaotic variability versus SST-forced predictability. *J. Climate*, **20**, 2251–2272, doi:10.1175/JCLI4070.1.

Stuart, N. A., and Richard H. Grumm, 2006: Using wind anomalies to forecast East Coast winter storms. *Wea. Forecasting*, **21**, 952–968, doi:10.1175/WAF964.1.

Trenberth, K. E., and J. M. Caron, 2000: The Southern Oscillation revisited: Sea level pressures, surface temperatures, and precipitation. *J. Climate*, **13**, 4358–4365, doi:10.1175/1520-0442(2000)013<4358:TSORSL>2.0.CO;2.